

## **Electronic Supplementary Information**

### **Flexible/Shape-Versatile, Bipolar All-Solid-State Lithium-Ion Batteries Prepared by Multistage Printing**

*Se-Hee Kim, Keun-Ho Choi, Sung-Ju Cho, JongTae Yoo, Seong-Sun Lee, and Sang-Young  
Lee\**

Department of Energy Engineering, School of Energy and Chemical Engineering, Ulsan  
National Institute of Science and Technology (UNIST), Ulsan 44919, Korea

Correspondence and requests for materials should be addressed to S.-Y. Lee (email:  
[syleek@unist.ac.kr](mailto:syleek@unist.ac.kr))

**Fig. S1** Shear rate-dependent viscosity and photographs (inset images) of the cathode pastes as a function of composition ratio. The cathode paste (LCO/C.B.(carbon black)/Gel Electrolyte = 69/7/24) failed to measure its rheological properties due to serious particle agglomeration.

**Fig. S2** Rheological properties and ionic conductivity of the GCE pastes as a function of the ratio of gel electrolyte/ $\text{Al}_2\text{O}_3$  nanoparticles. (a) Shear rate-dependent viscosity and photographs (inset images). The GCE paste (gel electrolyte/ $\text{Al}_2\text{O}_3$  = 20/80) failed to measure its rheological properties due to serious particle agglomeration. (b) Viscoelastic properties ( $G'$  and  $G''$ ) of the GCE pastes as a function of shear stress. (c) Ionic conductivity of the printed GCE films as a function of temperature.

**Fig. S3** EDS mapping area of Al and F elements in the printed GCE (shown in Figure 1b).

**Fig. S4** SEM morphology of the (ETPTA/PVdF-HFP = 75/25 (w/w)) semi-IPN film; the PVdF-HFP was selectively etched prior to the SEM analysis.

**Fig. S5** Change in the characteristic FT-IR peaks assigned to the acrylic C=C bonds ( $1610\text{--}1625\text{ cm}^{-1}$ ) of the ETPTA in the printed GCE before/after UV irradiation.

**Fig. S6** Change in the characteristic FT-IR peaks assigned to the acrylic C=C bonds ( $1610\text{--}1625\text{ cm}^{-1}$ ) of the ETPTA before/after UV irradiation: (a) printed LCO cathode and (b) printed LTO anode.

**Fig. S7** TGA profiles of the SWCNT-coated electrode active powders. (a) SWCNT-coated LCO. (b) SWCNT-coated LTO.

**Fig. S8** Comparison of the electronic conductivity between the pristine LTO and SWCNT-coated LTO.

**Fig. S9** Cross-sectional SEM image of the printed mono full cell (composed of an LTO anode, GCE layer and LCO cathode). (a) Before the cycle test. (b) After the 50<sup>th</sup> cycle

**Fig. S10** Charge-discharge profiles of the conventional LCO cathode and LTO anode at 25 °C, where a coin-type half cell (LCO cathode (or LTO anode)/(1M LiPF<sub>6</sub> in EC/DMC = 1/1 (v/v))-soaked PE separator/ lithium metal) was cycled at a fixed charge/ discharge current density of 0.1 C/ 0.1C in the voltage range from 3.0 to 4.2 V and from 1.0 to 2.5 V, respectively.

**Fig. S11** Cycling performances of the printed bipolar cells connected in series as a function of cell number (1 → 3 cells) at 25 °C, where the cells were cycled at a constant charge/discharge current density (0.1 C/ 0.1 C). (a) Charge/discharge profiles at 1<sup>st</sup>, 25<sup>th</sup> and 50<sup>th</sup> cycles. (b) Capacity retention as function of cycle number.

**Fig. S12** A video clip showing the safety robustness (cutting test) of the printed bipolar 2-stacked cell.

**Fig. S13** Video clips showing the safety robustness (nonflammability test) of the printed bipolar 2-stacked cell that was fabricated

directly on the curved roof of a miniature toy car. A control cell (consisting of an LCO cathode, LTO anode, carbonate-based electrolyte (1 M LiPF<sub>6</sub> in EC/DMC = 1/1 (v/v)) and PE separator)) was also tested for comparison.

**Table S1** Comparison of this work with the previously reported sulfide and oxide solid electrolytes.

**Table S2** Comparison of this work with the previously reported bipolar LIBs.

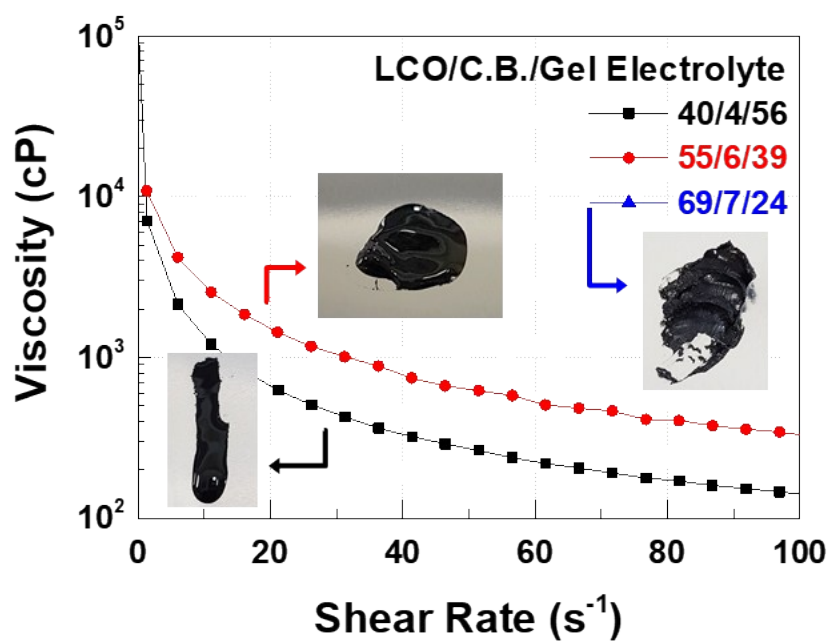


**Fig. S1** Shear rate-dependent viscosity and photographs (inset images) of the cathode pastes as a function of composition ratio. The cathode paste (LCO/C.B.(carbon black)/Gel Electrolyte = 69/7/24) failed to measure its rheological properties due to serious particle agglomeration.

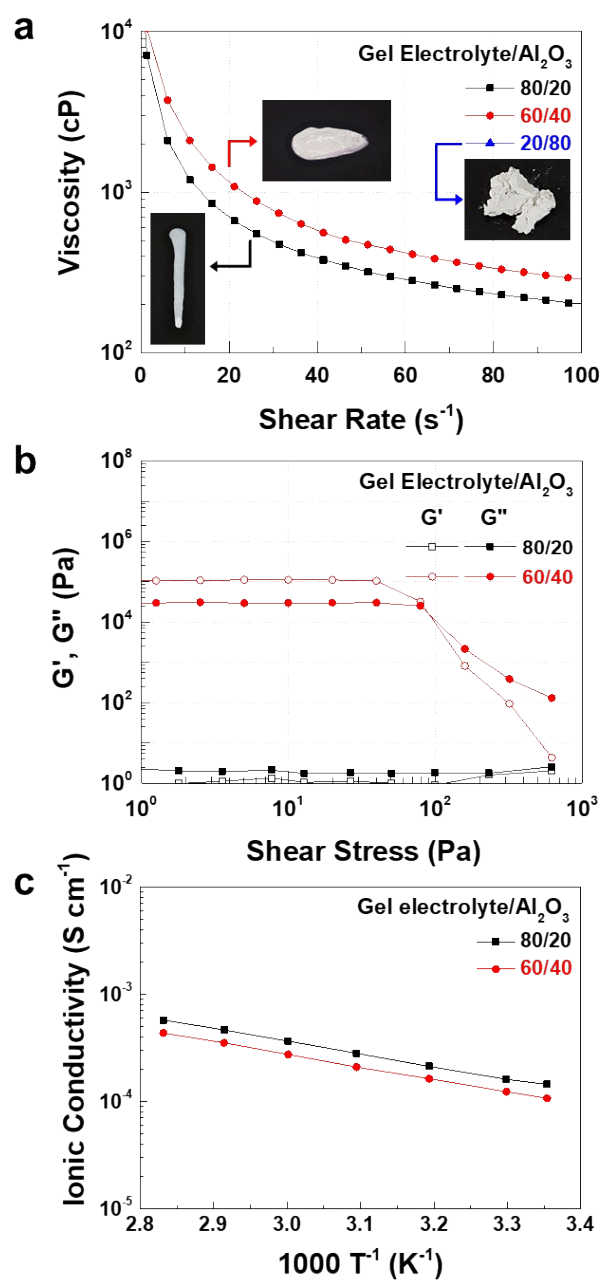


**Fig. S2** Rheological properties and ionic conductivity of the GCE pastes as a function of the ratio of gel electrolyte/ $Al_2O_3$  nanoparticles. (a) Shear rate-dependent viscosity and photographs (inset images). The GCE paste (gel electrolyte/ $Al_2O_3$  = 20/80) failed to measure its rheological properties due to serious particle agglomeration. (b) Viscoelastic properties ( $G'$  and  $G''$ ) of the GCE pastes as a function of shear stress. (c) Ionic conductivity of the printed GCE films as a function of temperature.

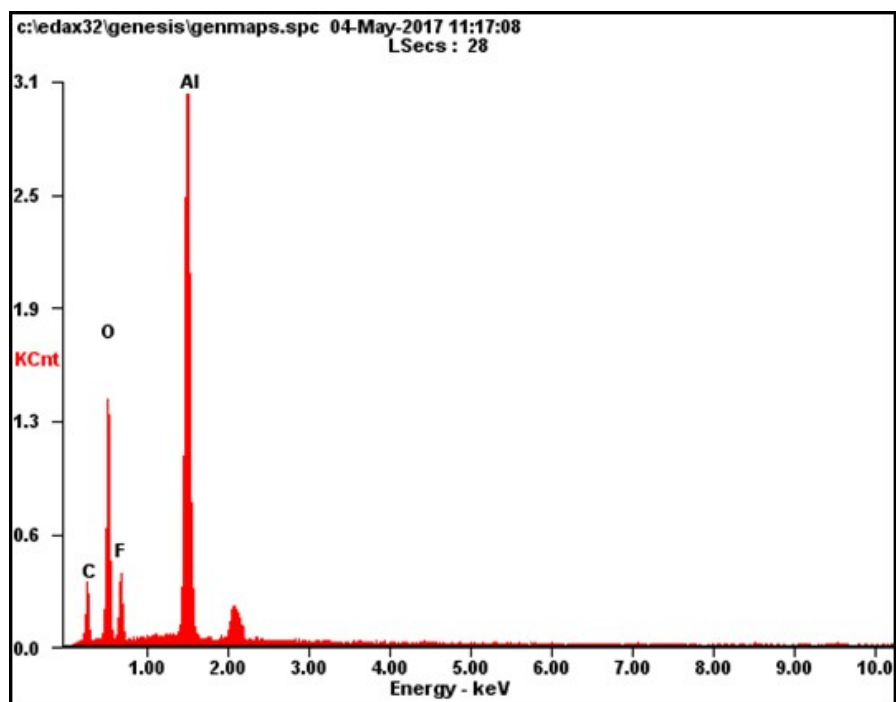


**Fig. S3** EDS mapping area of Al and F elements in the printed GCE (shown in Figure 1b).

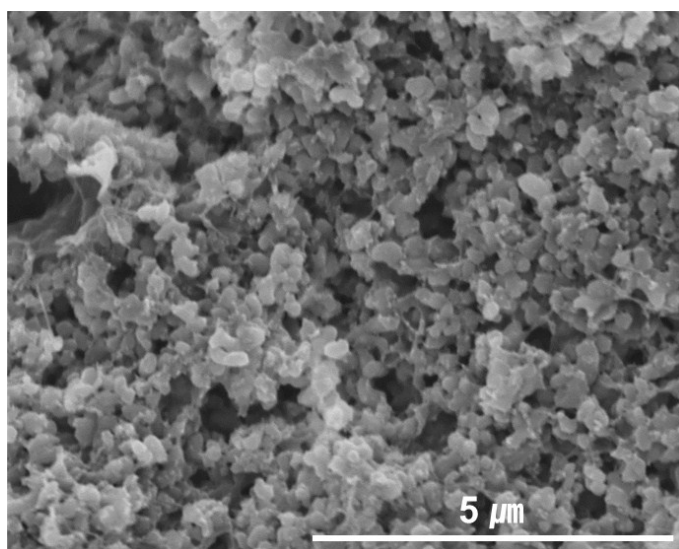


**Fig. S4** SEM morphology of the (ETPTA/PVdF-HFP = 75/25 (w/w)) semi-IPN film; the PVdF-HFP was selectively etched prior to the SEM analysis.



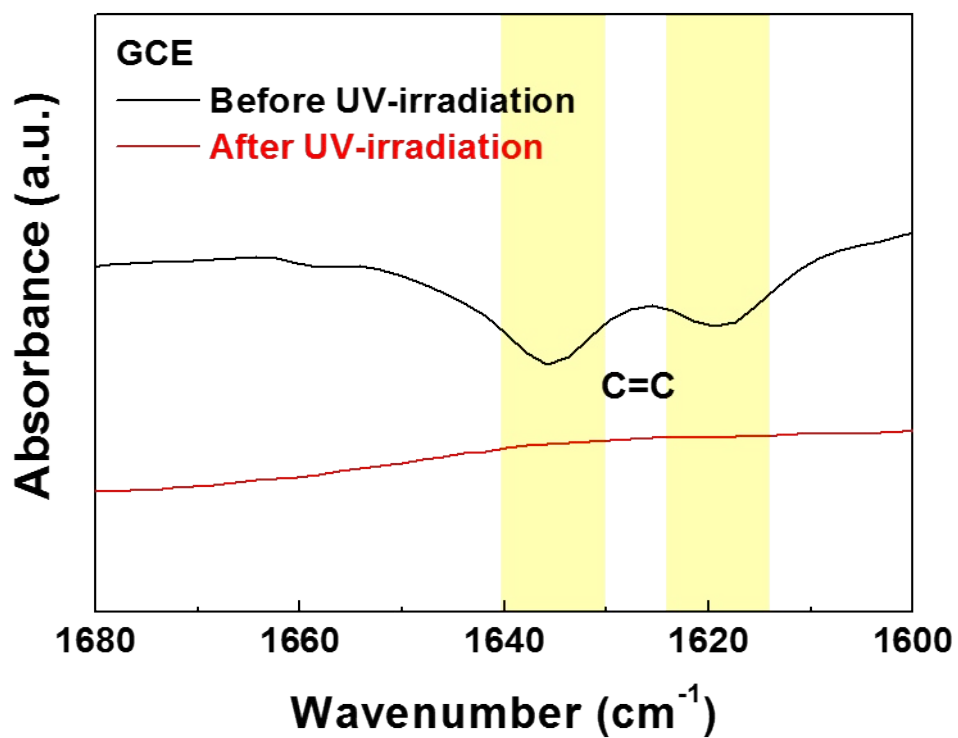


**Fig. S5** Change in the characteristic FT-IR peaks assigned to the acrylic C=C bonds (1610–1625 cm<sup>-1</sup>) of the ETPTA in the printed GCE before/after UV irradiation.

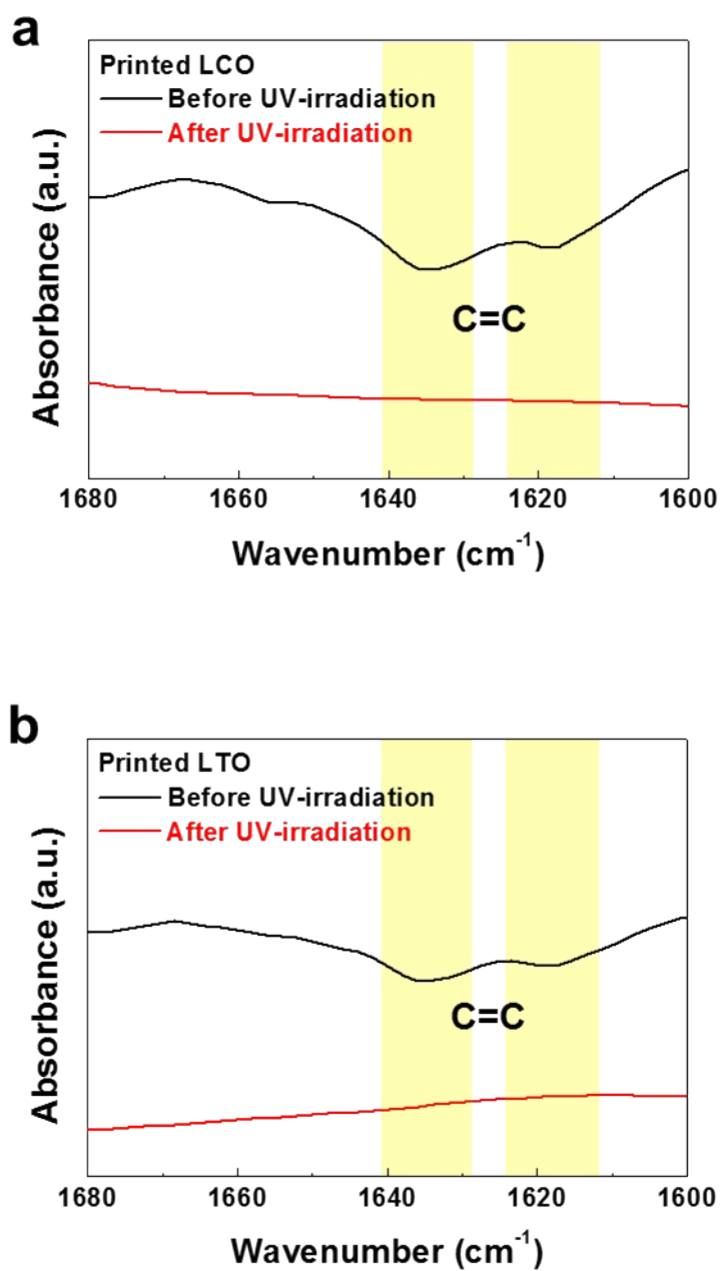


**Fig. S6** Change in the characteristic FT-IR peaks assigned to the acrylic C=C bonds (1610–1625  $\text{cm}^{-1}$ ) of the ETPTA before/after UV irradiation: (a) printed LCO cathode and (b) printed LTO anode.

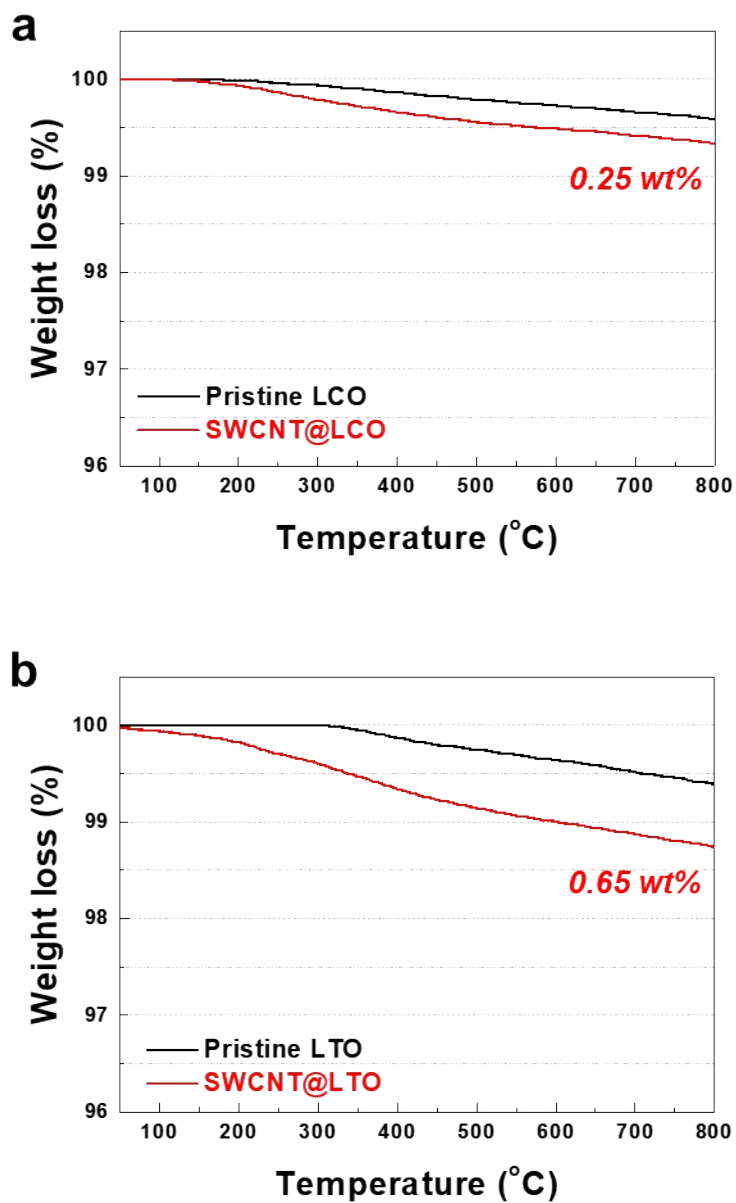


**Fig. S7** TGA profiles of the SWCNT-coated electrode active powders. (a) SWCNT-coated LCO. (b) SWCNT-coated LTO.

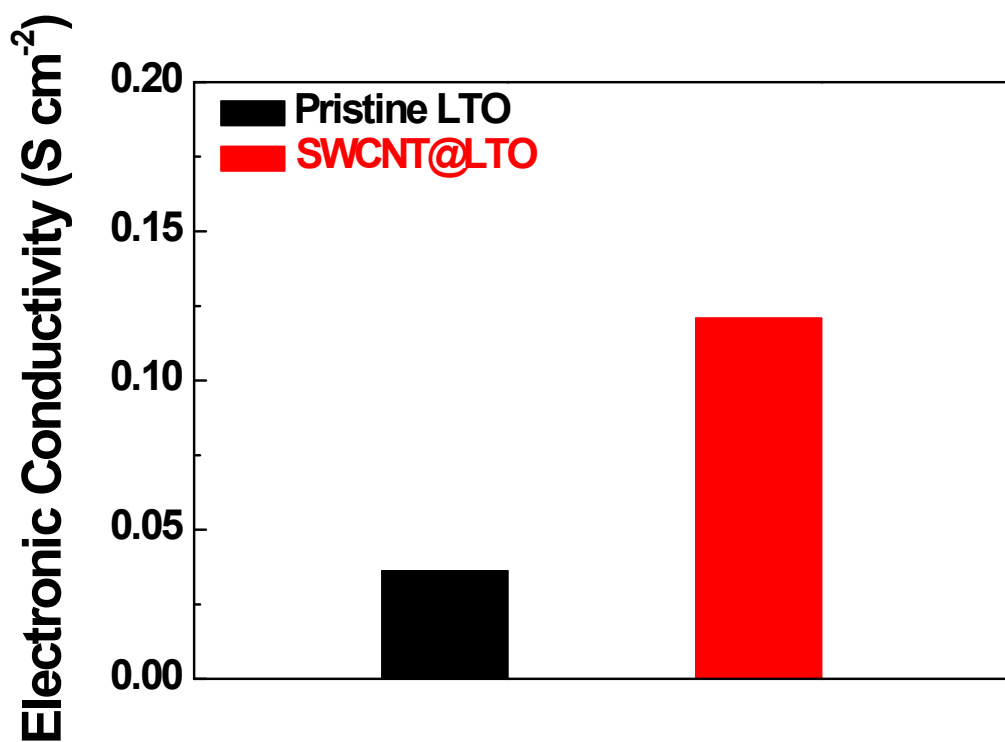


**Fig. S8** Comparison of the electronic conductivity between the pristine LTO and SWCNT-coated LTO.

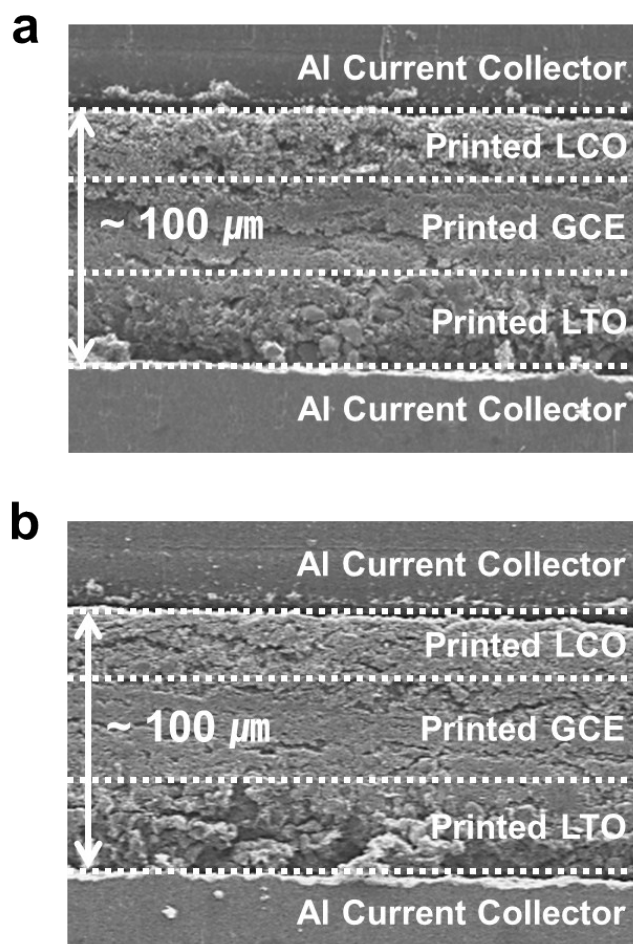


**Fig. S9** Cross-sectional SEM image of the printed mono full cell (composed of an LTO anode, GCE layer and LCO cathode). (a) Before the cycle test. (b) After the 50<sup>th</sup> cycle.

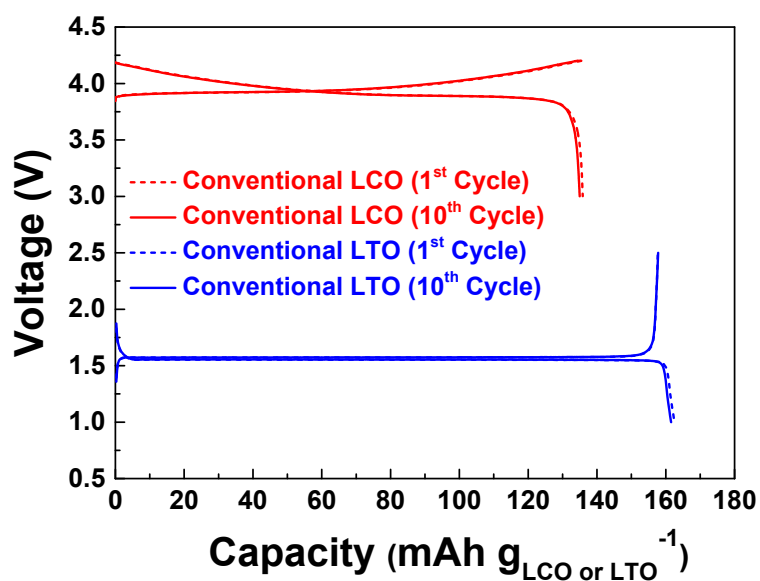


**Fig. S10** Charge-discharge profiles of the conventional LCO cathode and LTO anode at 25 °C, where a coin-type half cell (LCO cathode (or LTO anode)/(1M LiPF<sub>6</sub> in EC/DMC = 1/1 (v/v))-soaked PE separator/ lithium metal) was cycled at a fixed charge/ discharge current density of 0.1 C/ 0.1C in the voltage range from 3.0 to 4.2 V and from 1.0 to 2.5 V, respectively.

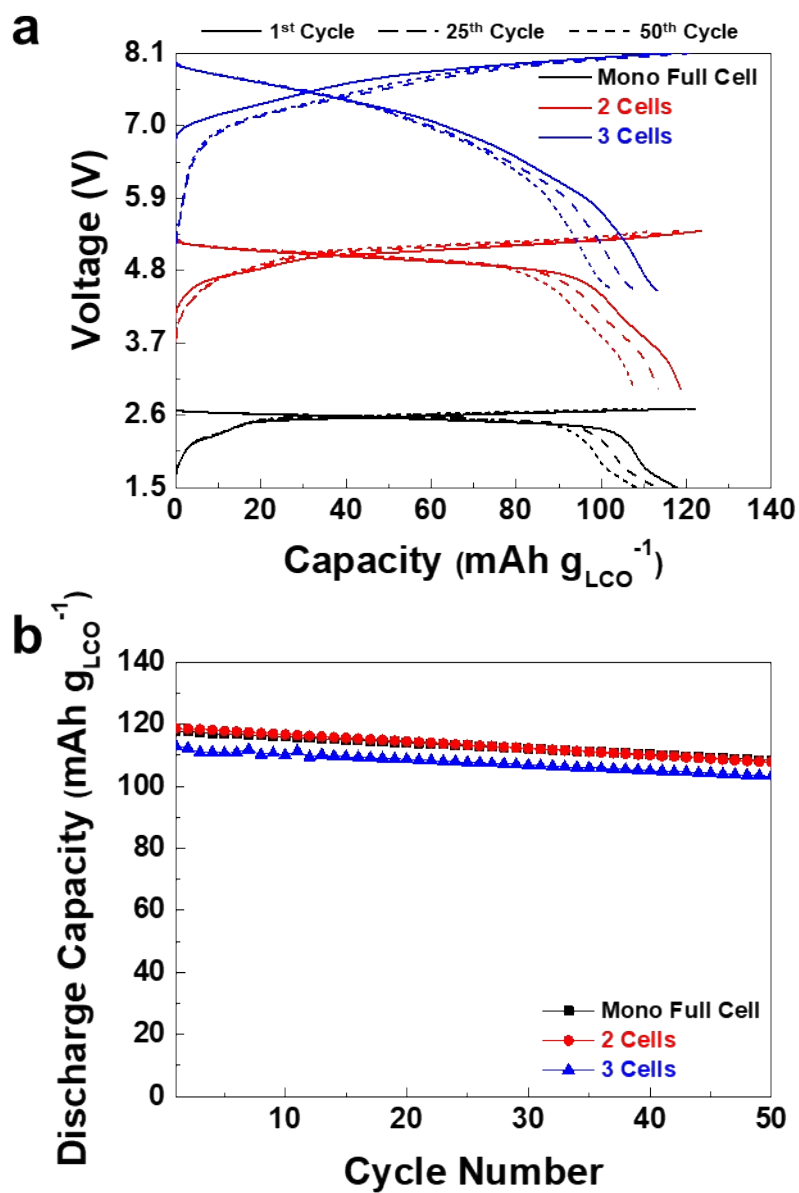


**Fig. S11** Cycling performances of the printed bipolar cells connected in series as a function of cell number (1  $\rightarrow$  3 cells) at 25 °C, where the cells were cycled at a constant charge/discharge current density (0.1 C/ 0.1 C). (a) Charge/discharge profiles at 1<sup>st</sup>, 25<sup>th</sup> and 50<sup>th</sup> cycles. (b) Capacity retention as function of cycle number.

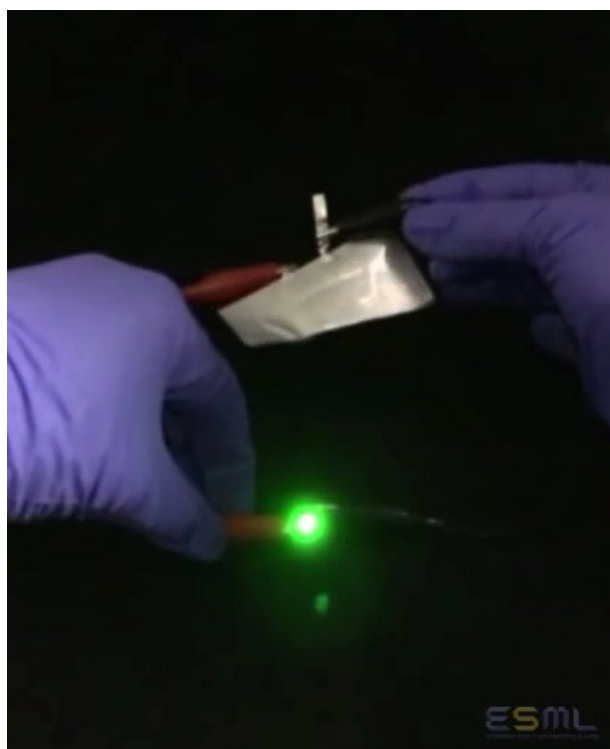


**Fig. S12** A video clip showing the safety robustness (cutting test) of the printed bipolar 2-stacked cell.



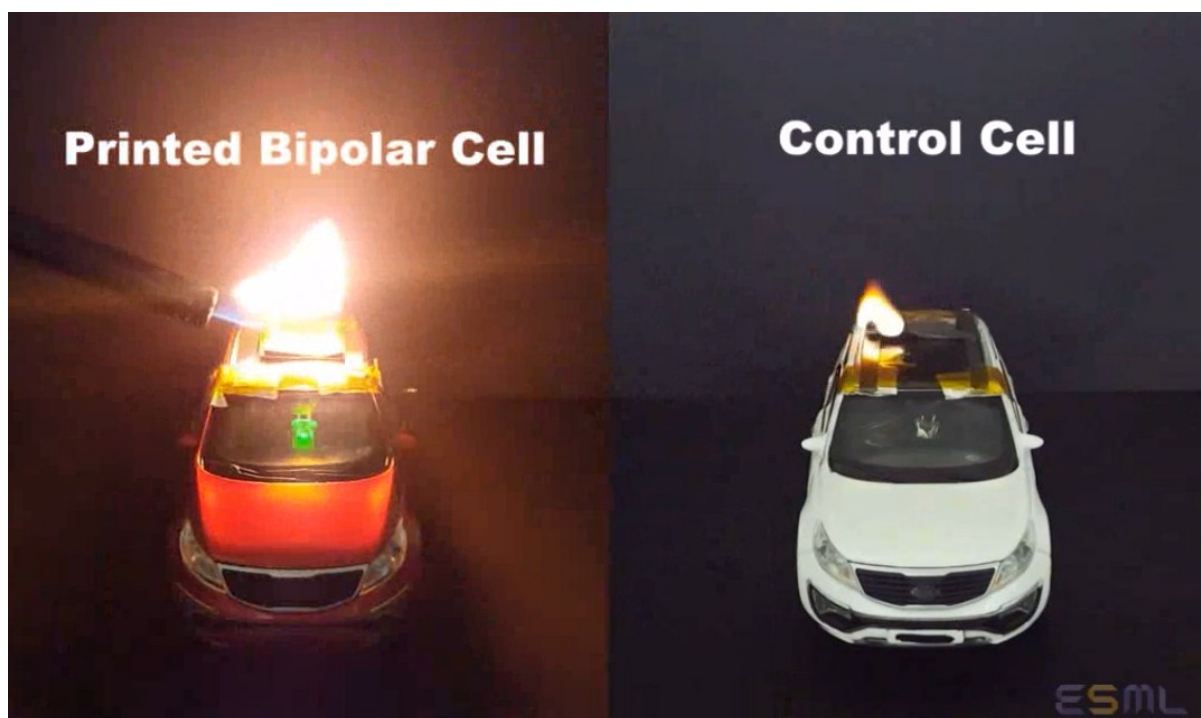


**Fig. S13** Video clips showing the safety robustness (nonflammability test) of the printed bipolar 2-stacked cell that was fabricated directly on the curved roof of a miniature toy car. A control cell (consisting of an LCO cathode, LTO anode, carbonate-based electrolyte (1 M  $\text{LiPF}_6$  in EC/DMC = 1/1 (v/v)) and PE separator)) was also tested for comparison.

Classification	Composition	Synthesis	Ionic Conductivity (S cm <sup>-1</sup> , R.T.)	Thickness (μm)	Flexibility	Safety	Shape Versatility	Ref.
GCE	1M LiBF <sub>4</sub> in SBN/ Semi-IPN/Al <sub>2</sub> O <sub>3</sub>	Printing/UV- Crosslinking (Room Temp., < 30 s)	10 <sup>-4</sup>	50	⊙	⊙	⊙	This work
Sulfide	Li <sub>2</sub> S-P <sub>2</sub> S <sub>5</sub>	Pelletizing (94 MPa, 280-300 °C for 2 h)	1.7 × 10 <sup>-2</sup>	-	-	⊙	-	S1
Sulfide	Li <sub>10</sub> GeP <sub>2</sub> S <sub>12</sub>	Pelletizing (30 Pa, 550 °C for 8 h)	1.2 × 10 <sup>-2</sup>	3000-4000	-	⊙	-	S2
Sulfide	Li <sub>9.54</sub> Si <sub>1.74</sub> P <sub>1.44</sub> S <sub>11.7</sub> Cl <sub>0.3</sub>	Pelletizing (240-550 °C)	2.5 × 10 <sup>-2</sup>	1000-2000	-	⊙	-	S3
Oxide (Perovskite)	La <sub>0.51</sub> Li <sub>0.34</sub> TiO <sub>2.94</sub>	Pelletizing (1350 °C for 6 h)	1.4 × 10 <sup>-3</sup>	-	-	⊙	-	S4
Oxide (Garnet)	Li <sub>7</sub> La <sub>3</sub> Zr <sub>2</sub> O <sub>12</sub>	Pelletizing (1230 °C for 36 h)	3.0 × 10 <sup>-4</sup>	980	-	⊙	-	S5
Oxide (NASICON)	Li <sub>1.3</sub> Al <sub>0.3</sub> Ti <sub>1.7</sub> (PO <sub>4</sub> ) <sub>3</sub>	Pelletizing (3 Mpa, 950-1000 °C for 24 h)	3.0 × 10 <sup>-3</sup>	1400	-	⊙	-	S6

**Table S1** Comparison of this work with the previously reported sulfide and oxide solid electrolytes.

# of Stacked Cells	Measurement Temp. (°C)	Cycle #	Safety	Flexibility	Ref.
3	25	50	☉	☉	This work
5	60	200	-	-	S7
2	30	1	-	△	S8
2	25	1	-	-	S9
2	39	200	-	-	S10
3	35	100	-	-	S11

**Table S2** Comparison of this work with the previously reported bipolar LIBs.

## References

- S1. Y. Seino, T. Ota, K. Takada, A. Hayashi and M. Tatsumisago, *Energy Environ. Sci.*, 2014, **7**, 627-631.
- S2. N. Kamaya, K. Homma, Y. Yamakawa, M. Hirayama, R. Kanno, M. Yonemura, T. Kamiyama, Y. Kato, S. Hama and K. Kawamoto, *Nat. Mater.*, 2011, **10**, 682-686.
- S3. Y. Kato, S. Hori, T. Saito, K. Suzuki, M. Hirayama, A. Mitsui, M. Yonemura, H. Iba and R. Kanno, *Nat. Energy*, 2016, **1**, 16030-16036.
- S4. M. Itoh, Y. Inaguma, W.-H. Jung, L. Chen and T. Nakamura, *Solid State Ionics*, 1994, **70**, 203-207.
- S5. R. Murugan, V. Thangadurai and W. Weppner, *Angew. Chem. Int. Edit.*, 2007, **46**, 7778-7781.
- S6. K. Arbi, J. Rojo and J. Sanz, *J. Eur. Ceram. Soc.*, 2007, **27**, 4215-4218.
- S7. K. Yoshima, Y. Harada and N. Takami, *J. Power Sources*, 2016, **302**, 283-290.
- S8. Y. J. Nam, S.-J. Cho, D. Y. Oh, J.-M. Lim, S. Y. Kim, J. H. Song, Y.-G. Lee, S.-Y. Lee and Y. S. Jung, *Nano Lett.*, 2015, **15**, 3317-3323.
- S9. T. Sato, T. Morinaga, S. Marukane, T. Narutomi, T. Igarashi, Y. Kawano, K. Ohno, T. Fukuda and Y. Tsujii, *Adv. Mater.*, 2011, **23**, 4868-4872.
- S10. T. Matsuo, Y. Gambe, Y. Sun and I. Honma, *Sci. Rep.*, 2014, **4**, 6084-6088.
- S11. Y. Gambe, Y. Sun and I. Honma, *Sci. Rep.*, 2015, **5**, 8869-8873.